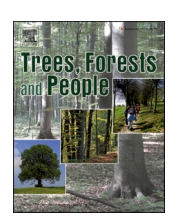
ELSEVIER

Contents lists available at ScienceDirect

# Trees, Forests and People





# Assessing the recovery of tropical forest structure, canopy closure and above-ground carbon during restoration: Comparing conventional with instrument-based metrics

Waiprach Suwannarat <sup>a,1</sup>, Stephen Elliott <sup>b,1</sup>, Worayut Takaew <sup>b</sup>, Pornpawee Laohasom <sup>b</sup>, Watit Khokthong <sup>a,b,\*</sup>

#### ARTICLE INFO

#### Keywords:

Forest ecosystem restoration Forest monitoring Forest carbon Forest structure Structural metrics Forest canopy cover

#### ABSTRACT

Carbon accumulation and structural development are key indicators of the progress of forest-ecosystem restoration. However current techniques of quantifying them are time-consuming, labor-intensive and costly. Therefore, we tested four instrument-based metrics (vegetation area index (VAI) from terrestrial LiDAR (light detection and ranging), leaf area index (LAI) from a plant-canopy analyser, and canopy cover, from both hemispherical photography (CC HP) and a densiometer (CC D)), as alternatives to conventional metrics (aboveground carbon (AGC), tree stocking density (TSD) and basal area (BA)), derived from manual measurements of trees. The study sites were: a control (pre-restoration conditions), 11/2- and 111/2-year-old forest, both undergoing restoration by the framework species method (FSM), and primary forest of indeterminate age (restoration target). VAI, LAI and CC\_D, clearly distinguished among the control site and 1½- and 1½-year-old-restoration (P < 0.05). CC\_HP failed to distinguish the control plot from young restoration. All four metrics correlated well (r =0.58-0.80) with conventional metrics (above-ground carbon (AGC), tree stocking density (TSD) and basal area (BA)), when data were combined across all plots, although plot-level correlations weakened, with increasing structural development. Furthermore, the instrument-based metrics failed to reflect a doubling in AGC between 111/2-year-old restoration and the reference forest, by under-estimating increases in structural development beyond canopy closure. CC D is recommended for monitoring structural development, during early forest restoration, due to its cost-effectiveness, ease of use and minimal disturbance of the forest understory. After canopy closure, AGC remains the most useful metric to gauge how closely restoration achieves reference-forest structure. After 11½ years of implementing the FSM, AGC had reached 49 % (65.9 tC/ha, ±SD 30.44) of the reference forest level (137.4 tC/ha,  $\pm$ SD 83.19).

# Abbreviations

AGB Above-ground biomass
AGC Above ground carbon
BA Stem basal area
CC Canopy cover

CC\_D Canopy cover from forest densiometer

CC\_HP Canopy cover from hemispherical photography

CT Non-planted control

DBH Tree diameter at breast height

DTM Digital terrain model EV Exposure value

FSM Framework species method GBH Tree girth at breast height HP Hemispherical photograph

LAI Leaf area index

LiDAR Light Detection and Ranging PCA Plant canopy analyser

R12 Restoration forest planted in 2012 ( $11\frac{1}{2}$  years old) R22 Restoration forest planted in 2022 ( $1\frac{1}{2}$  years old)

E-mail address: watit.khokthong@cmu.ac.th (W. Khokthong).

https://doi.org/10.1016/j.tfp.2025.100928

<sup>&</sup>lt;sup>a</sup> Environmental Science Research Center, Faculty of Science, Chiang Mai University, Chiang Mai, Thailand

b Forest Restoration Research Unit, Department of Biology, Faculty of Science, Chiang Mai University, Chiang Mai, Thailand

 $<sup>^{\</sup>star}$  Corresponding author.

<sup>&</sup>lt;sup>1</sup> These authors contributed equally to this work. Joint 1st authors.

RF Reference forest

TLS Terrestrial laser scanning
TSD Tree stocking density
VAI Vegetation area index

#### 1. Introduction

Throughout the tropics, efforts to restore forest ecosystems on degraded land are intensifying, as billions of trees are planted to combat biodiversity loss and to meet the ambitious targets of global and regional initiatives to tackle climate change (UN Decade on Restoration, n.d.; FAO, 2024). As evidence accumulates that restoring tropical forest ecosystems sequester carbon more rapidly than other land-use-change (LUC) solutions to climate change (Sacco et al., 2021; Jantawong et al., 2022), the need for more efficient and less intrusive monitoring, to verify such results, grows.

Forest restoration usually combines assisted natural regeneration (Shono et al., 2007) with tree planting, to recover ecosystem biomass, structural complexity, biodiversity and ecological functionality close to pre-disturbance levels. Both planted and naturally regenerating trees are subject to intensive maintenance (weeding and fertilizer application) over the first two years, to initiate canopy closure, after which, the ecosystem ideally becomes self-sustaining (Elliott et al., 2013). Progress towards achieving these goals requires frequent and accurate monitoring, so that subsequent restoration methods, including species selection and maintenance regimes, can be adjusted for optimum results. Such so-called "adaptive management" is well recognized as an essential component of ecological restoration (Gilmor, 2007).

Monitoring is conventionally performed by measuring tree heights (with a pole or clinometer) and tree girth at breast height (with tape measures). When combined with species-specific wood-density data (usually obtained from online databases (Zanne et al., 2009)), such ground-based measurements can be used to estimate above-ground tree carbon (AGC), using allometric equations (Chave et al., 2014; Liu et al., 2023; Pati et al., 2022). In northern Thailand, Pothong et al. (2022) developed such equations, specifically for the forest trees of the region.

Such field measurements are labor-intensive, often involving large teams of people, who can inadvertently trample young tree seedlings, which could impede the forest's future carbon-absorption capacity. Furthermore, these measurements are rooted in traditional productionforestry practices; they do not directly assess those tree components responsible for carbon absorption into the ecosystem via photosynthesis, i.e., the leaves and their arrangement in tree crowns. To anticipate future carbon-storage potential of forests undergoing restoration, it therefore makes sense to include forest-canopy metrics, as they are likely to be related to a forest's subsequent photosynthetic capacity. Canopy cover (CC) is one such metric; the proportion of forest floor that is covered by the amalgamation of tree crowns, which form the forest canopy (Jennings et al., 1999; Seidel et al., 2011). Some high-tech methods (e.g. LiDAR (light detection and ranging), hemi-spherical photography, canopy analyzers etc. (Beckschäfer, 2015; Chianucci et al., 2015; Dassot et al., 2011)) are currently being considered, to determine canopy metrics and other elements of forest structure. Such techniques are expensive and can only be used by expert specialists currently, rendering them inaccessible to community groups, non-governmental organizations etc. Therefore, it is necessary to consider whether such advanced technologies are accurate and cost effective, compared with conventional techniques.

Consequently, in this paper, we compare conventional tree measurements with four instrument-based methods, which focus on various forest-canopy metrics: (i) vegetation area index (VAI), from point clouds derived from terrestrial LiDAR (Suwannarat et al., 2024), ii) leaf area index (LAI) (Chianucci et al., 2015), using a plant canopy analyser, (iii) canopy cover from hemi-spherical photography (CC\_HP) (Beckschäfer, 2015) and (iv) canopy cover, using a forest densiometer CC\_D (Russavage et al., 2021). Our study also explored some of the limitations

of these techniques e.g. woody elements that obscure leaves, over- or under-exposed hemispherical photos and nonuniform distribution of points in LiDAR point clouds (Černý et al., 2019; Loffredo et al., 2016; Taheriazad et al., 2019).

We tested the hypothesis that forest canopy metrics, measured by the four instrument-based techniques listed above, could be used to monitor and differentiate states of restoration of upland evergreen-forest in northern Thailand.

#### 2. Materials and methods

#### 2.1. Study sites

Data were collected from 18th November to 17th December 2023 at Mon Cham viewpoint, near the village of Nong Hoi in Chiang Mai Province, northern Thailand (18° 56' 18.0' N, 98° 49' 16.7' E), at an elevation of 1300 m above sea level. The original vegetation of the site had been upland evergreen forest (Maxwell and Elliott, 2001), which had mostly been cleared and converted to agriculture in the 1960–70's, subsequently abandoned, and overgrown by herbaceous weeds and grasses. Four contrasting study sites were demarcated in close proximity to one another: i) remnant undisturbed forest (i.e. reference forest (Gann et al., 2019): RF), ii)  $11\frac{1}{2}$ -year-old restoration forest, planted with trees in 2012 (R12), iii)  $1\frac{1}{2}$ -year-old restoration forest, planted with trees in 2022 (R22) and iv) degraded land, dominated by herbaceous weeds, not planted with trees (control: CT) (Fig. 1).

The framework species method (FSM) had been applied in the two restoration sites. This method of forest-ecosystem restoration involves planting tree species that are characteristic of the reference forest, which also exhibit high survival and growth rates on exposed areas, and are able to inhibit herbaceous weed growth and attract seed-dispersing animals (by producing fruits or habitat structures at a young age) (Elliott et al., 2022). The FSM is known for rapid carbon accumulation, with above-ground tree carbon approaching that of reference forest within 20–30 years (Jantawong et al., 2017).

# 2.2. Conventional assessment of above-ground tree carbon using an allometric model and basal area

In each of the four study sites, eight circular sample plots of radius 5 m were established. Within each circle, the height (m) and girth at breast height (GBH (cm)) of all trees with GBH > 5 cm were measured. GBH was measured using a tape measure, whilst tree heights were determined using an extendable pole (for trees up to 10 m tall) or a clinometer (for trees taller than 10 m). GBH was converted to tree diameter at breast height (DBH) by dividing by pie.

The species of each tree was recorded by an experienced team of restoration ecologists and the species-specific wood density obtained either from Pothong et al. (2022) or from the Global Wood Density Database (Zanne et al., 2009). For species with multiple published values of wood density, the species mean was used. For non-listed species, genus means were used and for those without genus means, the mean value for all northern Thailand trees in Pothong's study was substituted (0.52 g/cm<sup>3</sup>).

The following allometric equation from Pothong et al.'s study of northern Thailand trees was used to estimate the above-ground biomass of each tree (Eq. (1)). We also applied an average carbon content value of 44.84 % (also reported by Pothong et al. for the trees of northern Thailand). Thus, the amount of carbon stored in each tree could be estimated using Eqs. (1) and (2).

Above – ground biomass(AGB) = 
$$a \times (DBH^2 \times H \times WD)^b$$
 (1)

Above – ground carbon (AGC) = 
$$0.4484 \times AGB$$
 (2)

... where, AGB is an individual tree's above-ground biomass (kg), DBH is

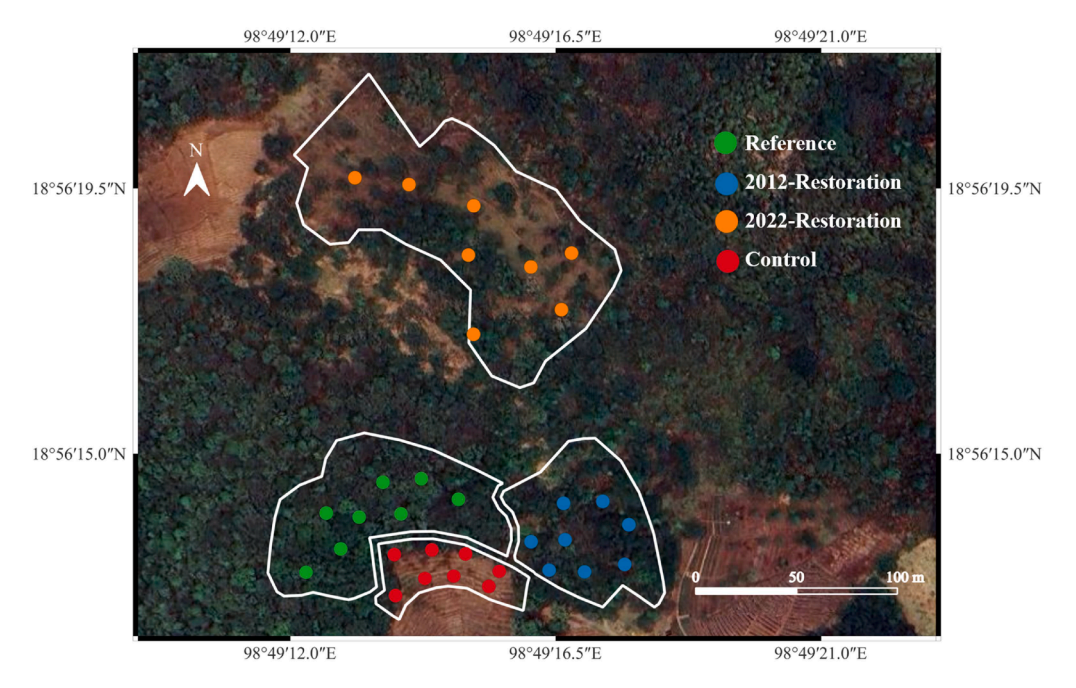


**Fig. 1.** Sample-plot locations at Mon Cham, within each of the four study sites: RF (the reference forest, 0.68 ha), R12 (restoration forest planted in 2012, 0.51 ha), R22 (restoration forest planted 2022, 1.26 ha) and in CT (non-planted control site, 0.23 ha). Interior views of the sites are presented in the supplementary materials (Figure S1).

tree diameter at breast height (cm) (GBH/pie), H is tree height (m) and WD is wood density (g/cm³). For trees of DBH=1.6 to 20.0 cm, the values used for the parameters 'a' and 'b' were 0.134 and 0.847, respectively. However, for trees of DBH>20.0 cm, the parameter values used were 0.067 and 0.976, respectively. Parameter values were empirically derived by Pothong et al. (2022), from felling and measuring 76 trees. AGC of all trees in each circle was summed, and the mean total/circle converted into an estimate of tons/ha for each of the four sites.

Basal area (BA) is a useful index of forest structure as it combines numbers of trees per unit area (tree stocking density, TSD) with their sizes. It is the proportion of a sample area occupied by the sum of the cross-sectional areas (1.3 m above ground) of all tree stems in the plot, expressed as  $m^2$  stems/ha (Bettinger et al., 2017). The stem

cross-sectional area of each tree was calculated from the GBH measurements, mentioned above (Eq. (3)):

$$BA_i = GBH^2 / \left(4\pi \times 10^4\right) \tag{3}$$

... where  $BA_i$  is individual tree stem basal area ( $m^2$ ), GBH is tree girth at breast height (cm). Individual-tree  $BA_i$  values were summed to derive the plot BA values in  $m^2$ /ha (Eq. (4)):

$$BA = \Sigma BA_i \times (10,000 / 78.5) \tag{4}$$

# 2.3. Vegetation area index (VAI) derived from LiDAR point clouds

In each of the same circular sample plots, a vegetation area index was derived from terrestrial laser scanning, using a FARO Focus Core LiDAR

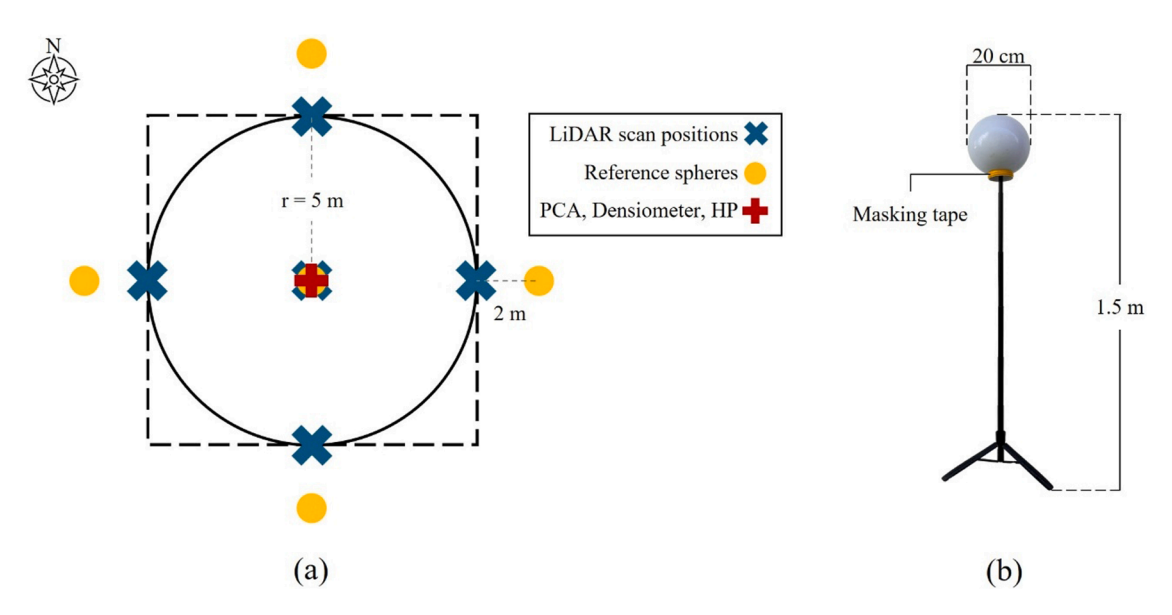


Fig. 2. (a) Setup for measurements in each 5-m radius sample plot. Measurements at the central point of each plot were made by light detection and ranging (LiDAR), plant canopy analyser (PCA), forest densiometer and hemispherical photography (HP). (b) One of the reference spheres used for merging LiDAR point clouds.

scanner (Faro Technologies, Inc., USA), mounted on a tripod, to acquire the 3-D structure of the forest as a point cloud. The scanner was set to 1/ 16 resolution and 4x scan quality (each point being scanned four times) in all sample circles. Color and texture were added to the point cloud from the parallel RGB camera. The scanner was controlled by an Apple iPad Air 3 (Apple Inc., 2018) via Wi-Fi. The scans were repeated in five positions in each circle: in the plot center and on the circular plot circumference in the due north, east, south and west positions (Fig. 2). This approach was recommended by Liang et al. (2016) to deal with the problem of trees obscuring each other within a single scan. To combine all five scans, into a single point cloud, five references spheres were placed in fixed positions in each of the sample plots, shown in Fig. 2a. These reference spheres were custom-made by placing a 20-cm sphere pole light (Luzino; Jewel P08-WH) on a 1.5-m camera stand (Fig. 2b). Furthermore, the reference spheres were marked with colored masking tape, to prevent confusion during merging the scans (scan registration).

All scan data in each plot were processed using Faro SCENE software (version 2023.1.0; Faro Technologies, Inc. USA). For merging the five point-clouds in each plot, we employed the manual registration method, using reference sphere identification (SCENE, 2022). During manual registration, the software positions each individual model into the main model one at a time.

At least two identical locations or objects (reference spheres in our case) must be spotted in each pair of scans (Fig. 3a). Typically, the mark sphere tool was used to locate the reference sphere. However, if the sphere was obstructed, the tool can fail to fully detect it. In such cases, a mark point was used to assign the reference spot on part of the sphere or surrounding area. After registration, the merged model was trimmed to a  $10~{\rm m}\times10~{\rm m}$  square, to fit the circles (5 m radius) used for AGC measurements. The point cloud was then exported in LAS format for VAI analysis. Raw and processed point cloud densities are presented in the supplementary materials (Table S1)

Model analysis involved (i) model preparation (Atkins et al., 2018) and (ii) index calculation (Taheriazad et al., 2019) (Fig. 4). Model preparation was performed using the lidR package (Roussel et al., 2020) in R language. First, a digital terrain model (DTM) was created, using the 'classify ground', 'filter ground' and 'rasterize terrain' functions, sequentially. The DTM was then subjected to height normalization, using the 'normalize height' function to flatten the ground. Then, points lower than 1.2 m were removed, to eliminate ground flora including small tree saplings. To remove noise, we used the 'stray points filter' function in the Faro SCENE software after the model registration. The distance threshold was set to 3 cm with the allocation threshold at 33.33 %.

VAI was then calculated from the processed 3D LiDAR point cloud

(Fig. 4). VAI is defined as the total surface area of all vegetation components (leaves, stems, branches, etc.) per unit ground area (a dimensionless proportion) (Atkins et al., 2018; Taheriazad et al., 2019). To calculate VAI, the number of points was observed within subsample boxes called "voxels". For the dimensions of each voxel see Eqs. (5) and (6).

Voxel dimension = 
$$\mathbf{u}_{(length)} \times \mathbf{u}_{(width)} \times \mathbf{D}$$
 (5)

... where u is  $10 \times \text{res}$  (mm) and D is the average width of the leaves (m).

$$res = \mathbf{R} \cdot \Delta \Psi \tag{6}$$

... where res is the model resolution (mm), R is the distance to the observed point (m), and  $\Delta\Psi$  is the angular resolution of the scanner (microradian, µrad).

Within each voxel, the number of points was limited to three, to address unevenness of point distributions. The approach to set a maximum threshold of 3 points. We used the 'length()' function to count the number of points in each voxel in the data frame. Then, an 'if...else' conditional to re-assign the point number count to '3' in any voxel exceeding three points. Subsequently, the total number of points in all voxels was multiplied by the average area of a single leaf, to calculate the VAI value of the model (Eq. (7)) (Taheriazad et al., 2019).

$$VAI = \frac{\text{No. of points} \times \text{Average single leaf area } (m^2)}{\text{Total ground area } (m^2)} \tag{7}$$

All model processing was done on a Victus 16 laptop (HP Inc., 2021) with AMD Ryzen 5 5600H CPU, NVIDIA GeForce RTX 3050 laptop GPU, and 16 GB DDR4 3200 MHz RAM.

#### 2.4. Leaf area index (LAI) using plant canopy analyser

A Li-Cor LAI 2200c (Li-Cor Biosciences, Inc., USA) plant-canopy analyser was used to measure LAI values in the sample plots. The scanner compares light conditions above the canopy—A (sky)—with those below it—B (target). Since our study employed a single optical sensor, the A readings were made using the 4A sequence shown in Table 1, to measure the average light conditions of the sky (K record).

To provide shade, the sensor was placed in the operator's shadow. All readings were done facing the same direction. How frequently the K record was made depended on sky conditions. For example, when the sky was clear and cloudless, the K record procedure was conducted hourly. However, when scattered clouds resulted in changeable sky conditions, the A and B measures were made in close succession.

The below-canopy B reading was made at the central point of each

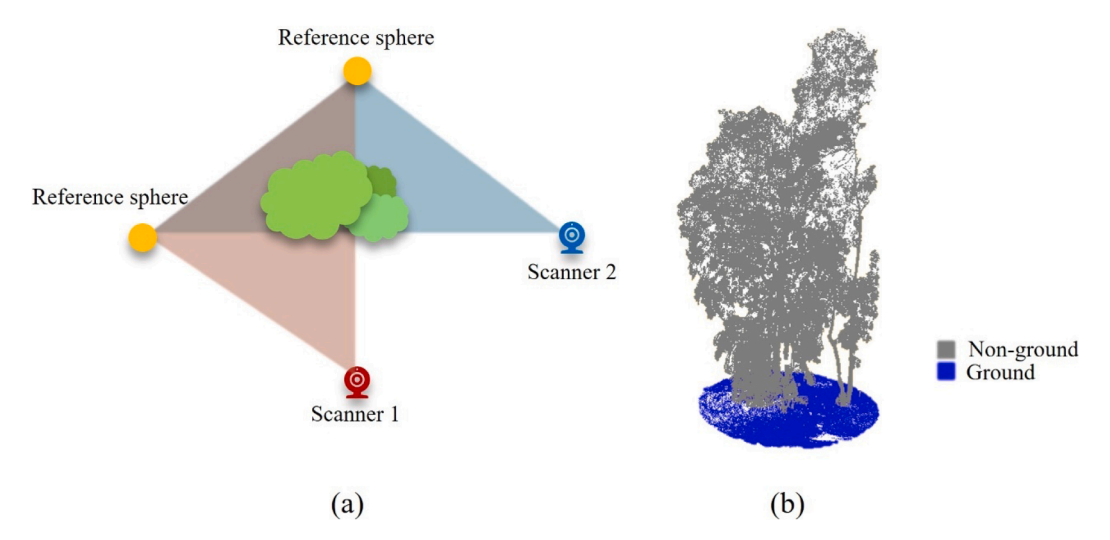
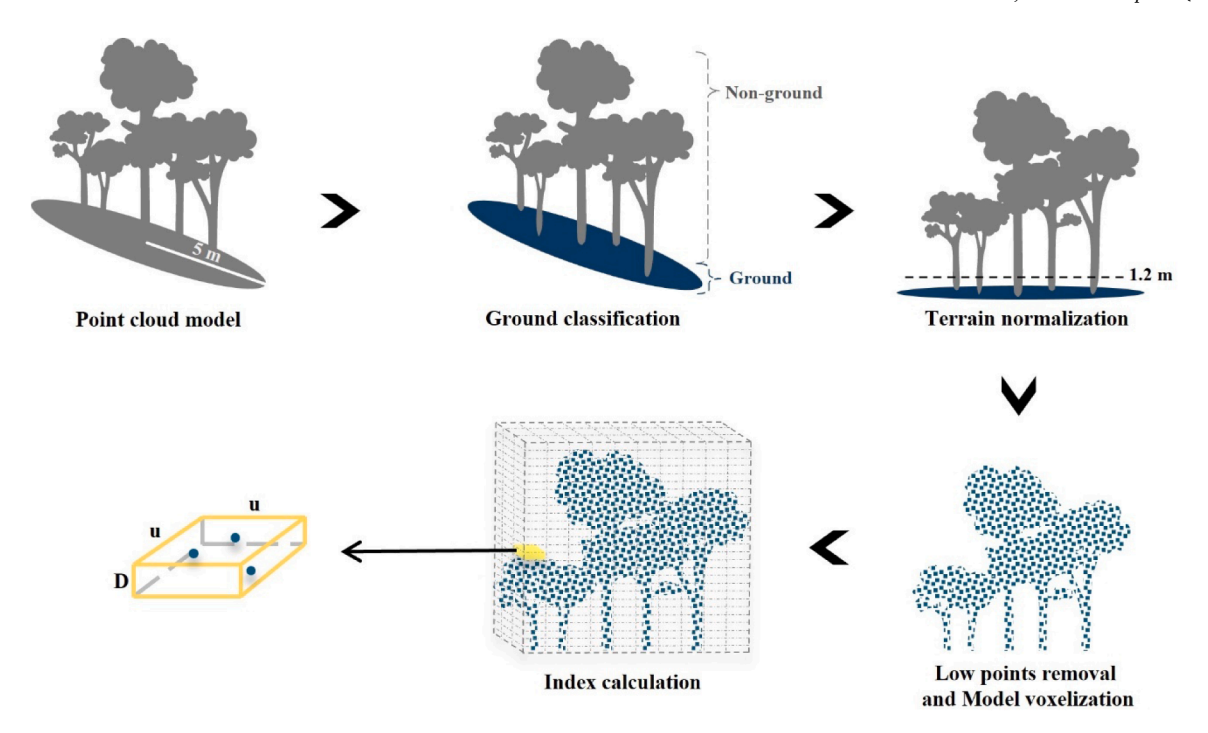


Fig. 3. (a) Two reference spheres spotted in both scan points of view. (b) the classified and flattened model.



**Fig. 4.** Workflow of VAI calculation from a point cloud model, obtained with a terrestrial LiDAR scanner. Upper; model preparation, lower; index calculations. Here, the yellow box is a voxel containing 3 LiDAR points (blue circles) of dimensions  $u \times u$  (ten times the resolution  $(10 \times \text{res}; \text{mm})) \times D$  (average width of the leaves (m)).

Table 1
Attachments and readings for the 4A sequence used to compile the K record.

Reading	Attachments			
#	Diffuser	Shade		
1	<b>√</b>	_		
2	✓	✓		
3	-	-		
4	_	✓		

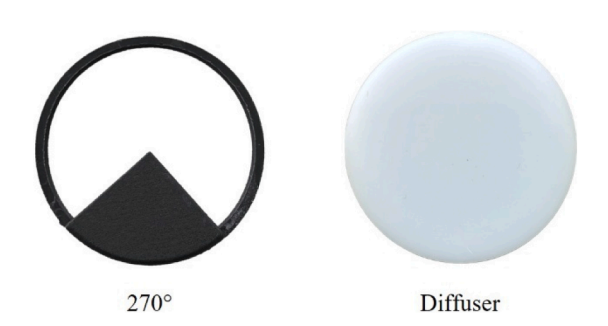


Fig. 5. View caps of plant canopy analyser.

sample plot, 1.2 m above the ground. Scans were done three times in each plot with the sensor facing north. All readings in every plot were performed with the  $270^{\circ}$  view cap on (Fig. 5) to avoid direct sunlight and the operator's shade. The time at which each reading was made was recorded for configuration during post-processing.

All readings from the LAI-2200c were imported into the FV2200 software (version 2.1.1; Li-Cor Biosciences, Inc., USA) via a USB cable. Corresponding K values were assigned with all configurations and parameters selected according to the sampling conditions and compared with B values to calculate LAI (Eqs. (8) and (9)).

$$T(\theta) = \frac{\text{Diffuse intensity below the canopy at view angle } \theta}{\text{Diffuse intensity above the canopy at view angle } \theta}$$
 (8)

... where  $T(\theta)$  is gap fraction of the given view angle (ring).

$$LAI = -2\sum_{i=1}^{5}ln(T(\theta_{i}))cos\theta_{i}\omega\ (\theta_{i}) \eqno(9)$$

... where  $\omega$  ( $\theta_i$ ) is the constant weight factor for each ring, and i refers to each of the detector rings with view angle centered at  $\theta_i$ .

#### 2.5. Canopy cover from hemispherical photography

Hemispherical photographs were taken with a digital camera (Fuji-film model X-E4; Fujifilm Corporation, Japan) fitted with a MEIKE 6.5 mm F/2.0 fisheye lens (Hongkong MEIKE Digital Technology Co., Ltd, China). The camera was attached to a tripod 1.2-m above the ground at the center of each sample plot, with the lens pointing direct upwards towards the zenith. The flash socket of the camera was always positioned in the north direction. The exposure values (EV) were incrementally reduced by 0.3 until no overexposed pixels were detected on the camera screen (Beckschäfer et al., 2013). Before every exposure, the operator positioned himself below the camera, to ensure that no extraneous elements are visible within the frame.

The photos were imported into ImageJ (version 1.48) (Schneider et al., 2012) and analyzed using the Hemispherical 2.0 plug-in (Beckschäfer et al., 2015) for canopy parameter analysis. The software converted raw hemispherical photographs (Fig. 6a) into black and white binarized photographs (Fig. 6b). Canopy cover was calculated as the percentage of white pixels in the binarized image.

#### 2.6. Canopy cover from forest densiometer

A spherical densiometer, model A, (Forest Densiometers, USA, Fig. 7a) was also used to quantify canopy cover in each sample plot. The instrument consisted of a convex mirror with a grid of 24 squares engraved upon its surface. To estimate canopy cover (CC), the instrument was leveled horizontally 1.2 m above the ground. Each square was divided into quarters in the mind's eye. The number of quarter-squares reflecting mostly sky was counted and multiplied by 1.04, to obtain an

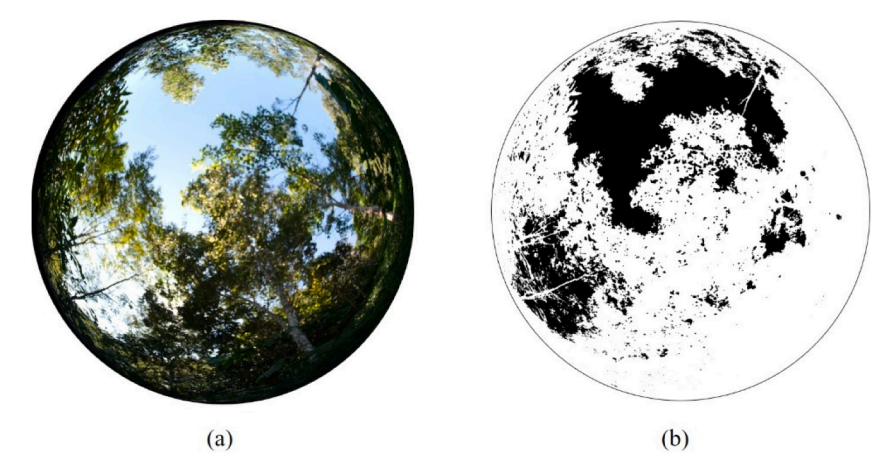


**Fig. 6.** (a) an input hemispherical photograph from the fisheye lens from the R22, 10th plot, captured on November 18, 2023; (b) the corresponding output binarized-hemispherical photograph for gap-fraction analysis (black = sky; white = canopy).

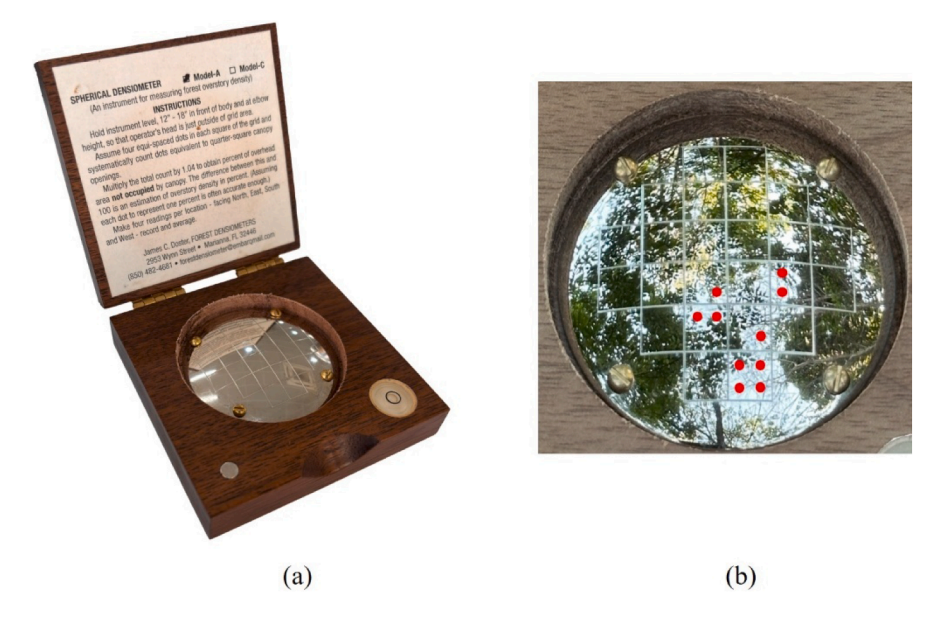


Fig. 7. (a) Forest densiometer model A, showing grid of 24 squares engraved upon the surface of a concave mirror; (b) example of forest densiometer quarter squares, reflecting mostly sky, counted—indicated by red dots: R12, 5th plot, taken on November 18, 2023.

estimate of the gap-fraction (GF) per cent (because there were 96 (not 100) quarter squares in the grid) (Fig. 7b). The gap-fraction per cent was subtracted from one hundred, to derive an estimate of the canopy-cover per cent (Eq. (10)). This was repeated four times in each sample plot (facing each of the cardinal points) and the values averaged.

$$CC = 100 - (GF \times 1.04) \tag{10}$$

... where CC is canopy cover (%) and GF is the number of quarter squares with visible sky. For example, Fig. 7b shows ten open quarter squares, corrected to 10.4 %. Therefore, the estimated canopy cover is 89.6 %. Images of the forest densiometer were captured from the sample plots with the operator's perspective, for future evaluation.

#### 3. Results

In thirty-two sample plots, mean values of all metrics, trended similarly across all four sites; from lowest values in the non-planted control site (CT), increasing sequentially from younger (R22) to older (R12) restoration sites, with maximum values attained in the reference forest (Tables 2 and S2).

Increases in mean VAI, LAI and CC\_D, between CT and R22 (control and  $1\frac{1}{2}$  year-old restoration), were significant (P<0.05, ANOVA) and substantial (per cent increases of 157, 131 and 1171 for VAI, LAI and CC\_D respectively, derived from Table 2). All metrics clearly distinguished between young and older restoration. Increases in all metrics between  $1\frac{1}{2}$  (R22) and  $11\frac{1}{2}$ -year-old restoration (R12)—both instrument-based and conventional—were significant (P<0.05) and substantial (per cent increases of 77.5, 115.0, 49.0, 45.4 for VAI, LAI, CC\_HP, CC\_D and 419.9, 149.0 and 335.0 for AGC, TSD and BA, respectively).

Comparing all metrics between R12 and the reference forest revealed how closely structural development of the  $11\frac{1}{2}$  year old restoration approached that of reference forest (RF). By  $11\frac{1}{2}$  years, mean values of instrument-based metrics in R12 had attained 89.6–97.7 % of reference-forest values (derived from Table 2), and the small differences between R12 and RF were statistically insignificant (P > 0.05). Considering the conventional metrics, mean TSD in R12 was 81.3 % of the RF value, whilst mean BA in R12 was 73.3 % of the RF value. Again, neither of these differences were statistically significant (P > 0.05), i.e. all instrument metrics, and two of the conventional metrics (TSD and BA) did not clearly distinguish between advanced restoration and the reference

Table 2
Mean metric values and one-way ANOVA results from each sampling site. CT; non-planted control, R22; restoration forest planted in 2022, R12; restoration forest planted in 2012 and RF; reference forest. VAI=vegetation area index; LAI=leaf area index; CC\_HP and CC\_D are canopy cover by hemispherical photography and densiometer, respectively; AGC=above-ground carbon; TSD= tree stockings density and BA= basal area.

Conventional measurements Instrument-based measurements VAI CC D TSD LAI CC HP AGC BA Site Mean + SD Mean ± SD Mean ± SD Mean ± SD Mean + SD Mean + SD Mean ± SD  $(m^2/ha)$ (%)(%) (tC/ha) (stems/ha)  $0.370^{a} \pm 0.45$  $0.765^{a} \pm 1.08$  $52.073^{a} \pm 10.50$  $4.840^{a} \pm 10.39$  $0.000^{a} \pm 0.00$  $0.000^{a} \pm 0.00$  $0.000^{a} \pm 0.00$ CT  $0.950^{b} \pm 0.49$  $1.771^{b} \pm 1.23$  $61.520^{b} \pm 29.32$  $12.668^{b} \pm 13.38$  $780.255^{b} \pm 516.05$ **R22**  $57.260^{a} \pm 19.20$  $7.850^{b} \pm 6.77$ R12  $1.686^{\circ} \pm 0.27$  $3.807^{c} \pm 0.90$  $85.299^{b} \pm 5.64$  $89.470^{\circ} \pm 5.26$  $65.866^{\circ} \pm 30.44$  $1942.675^{\circ} \pm 552.13$  $34.146^{\circ} \pm 13.41$  $1.725^{\circ} \pm 0.10$  $4.246^{\circ} \pm 0.37$  $92.977^{b} \pm 1.29$  $93.630^{\circ} \pm 1.96$  $137.451^{d} \pm 83.19$  $2388.535^{\circ} \pm 1043.28$  $46.549^{\circ} \pm 24.36$ RF

FOREST DEVELOPMENT

Values not sharing the same superscript are significantly different among sites (P < 0.05).

forest. Only AGC, was significantly lower in the R12 site than in the reference forest, attaining 47.9 % of the reference-forest value (in  $11\frac{1}{2}$  years) (P < 0.05).

Fig. 8a presents correlation coefficients (r), indicating the strengths of the relationships between the metrics, across all 32 plots. Most of the metrics were highly correlated with one another. Considering how well instrument-based metrics (VAI, LAI, CC\_HP and CC\_D) indicate conventional ones (AGC, TSD and BA), correlations between AGC and instrument-based metrics were moderate, with CC\_HP having the strongest relationship (r=0.67). However, the relationships between AGC and the other instrument-based metrics were only very slightly weaker (VAI, r=0.64; LAI, r=0.63 and CC D, r=0.58)

Correlations between TSD and instrument-based metrics were all stronger. The strongest relationship was with LAI (r=0.80), but it was only marginally stronger than the relationships between TSD and the other three instrument-based metrics. Correlations of instrument-based metrics with BA were also strong. The strongest relationship was with CC\_HP (r=0.75), which was only slightly stronger than with the other instrument-based metrics.

In contrast, within each of the four individual study sites, correlation coefficients, based on eight circular sample plots in each (Fig. 8b-e), were generally weaker and somewhat erratic. Since no trees were present in the sample plots in CT, no correlations between instrument-based metrics and conventional metrics could be derived (Fig. 8b).

In the young restoration plot (R22), the instrument-based metrics, which had the strongest relationships with conventional metrics, were CC\_HP and LAI with TSD (r=0.71 and 0.65 respectively) and VAI with AGC (r=0.63) (Fig. 8c). In the older restoration plot (R12), the strongest correlations between instrument-based and conventional metrics were between VAI with AGC (r=0.67) and BA (r=0.55) (Fig. 8d). In the reference forest, correlations were weaker. CC\_HP correlated most strongly with BA (r=0.42) (Fig. 8e). Other correlations between instrument-based and conventional metrics were much weaker.

#### 4. Discussion

This study compared instrument-based metrics (VAI, LAI, CC\_HP, and CC\_D) with conventional metrics, derived from direct, manual, tree measurements (AGC, TSD and BA), to monitor forest structural recovery during restoration by the framework species method (FSM) (Elliott et al., 2022). The relative advantages and disadvantages of all seven metrics investigated are summarized in Table 3. The study also demonstrated the extent of development of forest structure achievable over the first decade after implementing the FSM.

## 4.1. Instruments and metrics

Information content of the instrument-based metrics increased from

CC\_D and CC\_HP (degree of canopy closure), to LAI (canopy density including beyond initial canopy closure) and VAI (canopy physical structural complexity — including leaves and branches etc.).

#### 4.1.1. LiDAR and VAI

The advantage of terrestrial LiDAR is that it physically scans all forest structures (including leaves and branches) and combines them all into a single index—in this case VAI. Thus, the information content of the derived metric is much higher than that of the other instrument-based metrics in this study. Although the technique registered a non-zero value for the control plot (due to tall weeds and occasional shrubs), it clearly distinguished differences in structural development between the CT, R22 and R12 plots, but not between the R12 and RF plots (Table 2). VAI also correlated well with all conventional metrics, when considering the combined data from all plots (Fig. 8a).

However, the method appeared to underestimate forest structural development in RF. VAI values in R12 and RF were statistically indistinguishable, whereas AGC in R12 was, significantly, less than half that of RF. A problem with using terrestrial LiDAR in dense forest is that low branches and other close objects can block scanning of more distant structures, particularly those in the canopy (Liang et al., 2016; Torralba et al., 2022). This may have reduced the VAI in RF, such that the difference in mean VAI's between R12 and RF was less than expected, when compared with the difference in AGC measurements. It might also explain the low correlation coefficients between VAI and the conventional metrics in both R12 and RF (Fig. 8d & e).

In an attempt to address this issue, we combined five scans per plot (Fig. 2), since previous researchers have shown that using multiple scans (3-5) improves accuracy of the technique, compared to a single scan (Torralba et al., 2022). Despite this, under-estimation of VAI in RF was still apparent at the 1/16 resolution and 4x scan quality, used for this study. Higher resolutions should therefore be tested in the future, although high-resolution scanning considerably increases the fieldwork time needed. In contrast, Ehbrecht et al. (2017) successfully used single scans to generate the newly developed "stand structural complexity index" (SSCI), which holistically quantifies the spatial arrangement of plant material in forests. Furthermore, combining terrestrial and airborne LiDAR point clouds, has recently generated some impressive results for capturing forest structure, under various environmental conditions (Zhang et al., 2023). Therefore, we recommend further studies on the effects of scanning configuration and resolution, and on combining terrestrial and aerial LiDAR point clouds.

Considering the practicalities of using LiDAR for monitoring forestrestoration progress, setting up the tripod in five locations within 10m-diameter circles resulted in considerable trampling of tree saplings in the undergrowth, which may have affected subsequent forest regeneration. The instrument, the reference spheres and their tripods are bulky, and great care must be taken when transporting them and setting

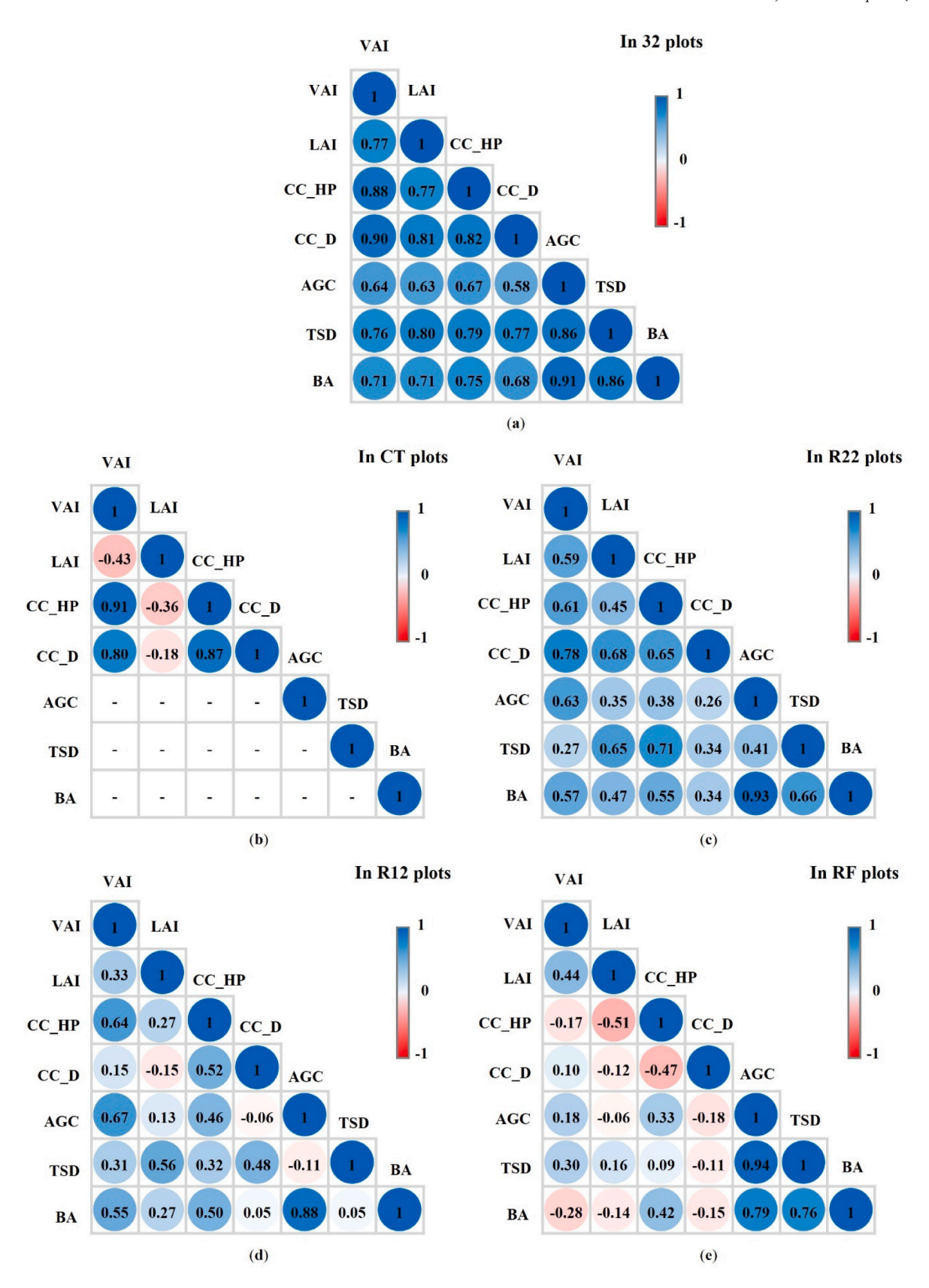


Fig. 8. Correlation coefficient (r) matrices among metrics; four instrument based: vegetation area index (VAI) from terrestrial laser scanning, leaf area index (LAI) from a plant canopy analyser (PCA), and canopy cover from hemispherical photography (CC\_HP) and a densiometer (CC\_D), and three conventional: above ground tree carbon (AGC), tree stocking density (TSD) and basal area (BA): (a) for all 32 plots combined across all 4 study sites and (b-e) for 8 plots in each of the sites (b) CT=control, (c) R22=forest restoration planted 2022 (1½ years old), (d) R12=forest restoration planted 2012 (11½ years old) and (e) RF=reference forest (least disturbed evergreen forest).

**Table 3**The pros and cons of four instrument-based and three conventional metrics for tracking progress of forest-structure development during forest-ecosystem restoration.

							• •
Method	Metric	Cost	Labour required	Time needed	Trampling risk	Advantages	Disadvantages
LiDAR	Vegetation area Index (VAI)	Very high (equipment)	Moderate	High ≅ manual survey	High if multiple scans	Direct scanning of all forest structures	Bulky. Complicated set-up. Steep learning curve. Obstruction by low objects may necessitate multiple scans.
Plant canopy analyser	Leaf area index (LAI)	Moderate	Low	Moderate	Moderate	Takes into account increases in canopy density beyond canopy closure. Compact.	Only considers leaf canopy. Frequent open-sky readings are needed when there are scattered clouds.
Hemispherical camera	Canopy cover (CC_HP)	Moderate	Low	Moderate	Low to moderate	Compact. Objective and precise.	Fiddly set-up and exposure settings. Disregards multiple leaf layers beyond canopy closure. Saturates at 100 %.
Densiometer	Canopy cover (CC_D)	Low	Low	Low	Low	Very compact and lightweight.	Subjective readings. Disregards multiple leaf layers beyond canopy closure. Saturates at 100 %.
Conventional forest survey	Above-ground carbon (AGC) Tree stocking density (TSD) Basal area (BA)	High (labour/ transport)	High	High	Very high	Well-established direct measurements. All derived from the same dataset. Results are comparable with other studies. Cheap materials and equipment.	High cost due to high labour/ transport requirements. Does not include canopy measurements.

them up. Post-processing of point clouds involves a steep learning curve. Crucially, terrestrial LiDAR scanners are very expensive (30,000–100,000 USD). The prospect of routinely using them to verify carbon credits, for example (Suwannarat et al., 2024), seems remote, until they become more affordable and user-friendly.

#### 4.1.2. Plant canopy analyser and LAI

A plant canopy analyser uses algorithms to infer an index of canopy density indirectly from the attenuation of light, as it passes through the forest canopy; it does not register forest structure directly, like LiDAR does. An LAI of <1 indicates incomplete canopy closure; "1" indicates cover by a single layer of leaves (on average); "2" by a double layer of leaves—and so on. Even after complete canopy closure, differences in light readings between the open sky and beneath the forest canopy should increase further, with increasing canopy density, i.e. the metric should not saturate at 100~% canopy cover.

LAI and VAI results were similar, in that LAI registered a non-zero value in the control plot, due to tall herbaceous weeds and shrubs, and it clearly distinguished differences in canopy development between the CT, R22 and R12 plots, but not between the R12 and RF plots (Table 2). Similarly, LAI also correlated well with all conventional metrics, when considering the combined data from all plots (Fig. 8a). As with VAI, however, the failure of LAI to distinguish between advanced restoration (R12) and the reference forest (RF), did not reflect the more than doubling of AGC between the two sites. Furthermore, correlations with conventional metrics in the denser plots (R12 and RF) were poor. Therefore, it seems that further increases in the canopy density, after canopy closure, are poorly related with further light attenuation.

Costing around 1000–15,000 USD, plant canopy analyzers are cheaper than LiDAR. They are easier to deploy than LiDAR, and can be used by a single observer, thus minimizing trampling of young tree seedlings. However, the need to make frequent open-sky readings (using a single sensor device) imposes difficulties. If the below-canopy sample points are far from the forest edge, the time interval between open-sky and under-canopy readings becomes unacceptably long, particularly when cloud conditions are changeable. This highlights the difficulty of using a passive-sensor device under variable ambient light conditions.

#### 4.1.3. Canopy cover

Both the hemispherical camera and the densiometer measure canopy cover (CC) by subtracting the amount of visible sky from a ground-up view of the forest canopy and assigning remaining pixels as "canopy".

Once no sky becomes visible (i.e. complete canopy closure), however, they return a CC of 100 %, no matter how many additional layers of leaves and branches grow and augment canopy density thereafter (Dassot et al., 2011; Huete et al., 2012; Pretzsch et al., 2019). The pattern of CC\_D results was the same as those of VAI and LAI. The metric returned a non-zero value for the control plot and distinguished between the CT, R22 and R12 plots, but not between the R12 and RF plots (Table 2). It also failed to reflect the doubling of AGC between R12 and RF. CC\_D correlated similarly well with the conventional metrics across all plots (Fig. 8a). Once again, correlations with conventional metrics in the denser plots (R12 and RF) were mostly very low (except for TSD in R12, r = 0.48) (Fig. 8d).

Hemispherical photography registered an obvious anomaly—52.1 % canopy closure in the control site (CT), where no trees grew (compared with 4.8 % from the densiometer) (Table 2). Although the camera's exposure value (EV) was manually adjusted, to prevent over- or underexposure (which may lead to errors in the CC estimation), the camera still included trees at the edge of the plot in images, due to the steep slope and the wide field of view of the hemispherical lens (zenith angle =  $90^{\circ}$ ) (Figure S3). To mitigate this in the future, hemispherical photos should be analyzed by other methods with smaller zenith angles, such as Can-Eye software (zenith angle =  $60^{\circ}$ ), to identify vegetation cover on steep terrain with more certainty (Khokthong et al., 2019; Weiss and Baret, 2017).

In common with all other instrument-based metrics CC\_HP was significantly higher in R12 than in R22, but the metric failed to distinguish between R12 and RF. As with other instrument-based metrics, correlations with conventional metrics weakened as structural development increased (Fig. 8c-e).

The main difference between the two canopy-cover instruments is that hemispherical photography employs a precise, objective procedure to subtract sky pixels from an image, whereas readings from a densiometer are more subjective, particularly if the instrument and viewing angle are not perfectly steady. However, a densiometer can be operated by non-skilled personnel, as it simply involves counting spots on a grid. In contrast, set-up and operation of a hemispherical camera are highly technical, and post processing images requires considerable expertise and training. Furthermore, hemispherical cameras are more expensive (1200–1500 USD) than densiometers (200–300 USD).

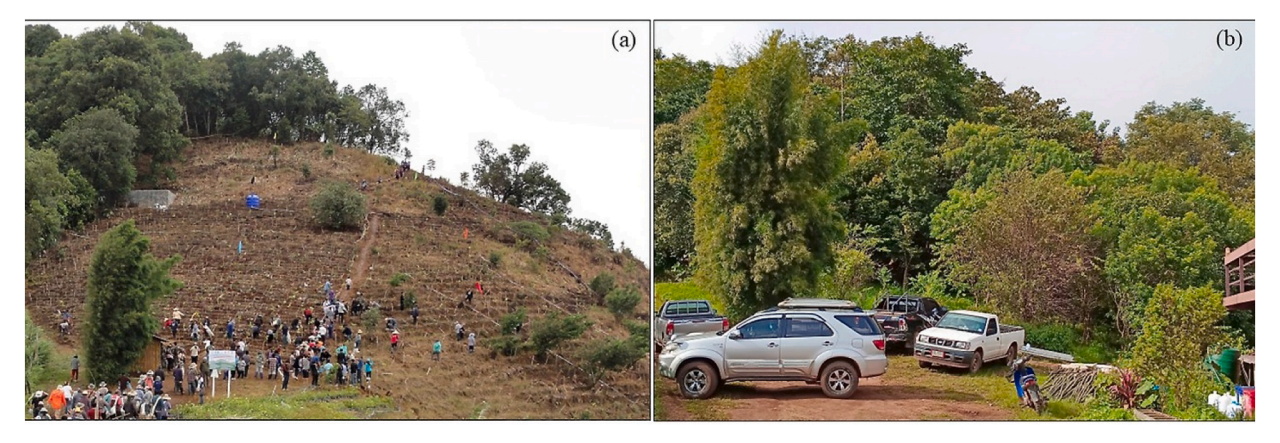


**Fig. 9.** (a) Initial conditions at the R12 restoration site on planting day (28/07/2012), with the edge of the adjacent reference forest (RF) visible top left. Note the landmark bamboo clump lower left. (b) A closer view of the same site 11½ years later (08/11/2023). The restored forest (to the right) is almost indistinguishable from the reference forest (to the left) (Photos: Stephen Elliott).

#### 4.2. Conventional forest surveys

All conventional metrics were obtained from the same manual measurements of trees of GBH>5 cm in all circular sample plots, using standard, survey techniques, carried out by teams of 5–6 people. The information content of the metrics increased from TSD (tree counts) to BA (tree counts and tree sizes (GBH)) and AGC (tree counts, sizes (GBH and height) and wood density).

Structure is built from biomass, of which 45 % is carbon (Eq. (2)). Therefore, as AGC increases, so should the structural complexity of the forest, as the carbon becomes partitioned among an increasing diversity of structural components. This should have been reflected by strong correlations of AGC with instrument-based metrics of structural development. In general, correlations of AGC with instrument-based metric were moderate, becoming weak in the R12 and RF plots. This may have been because calculation of AGC is sensitive to wood density (Eq. (1)), a variable which was "invisible" to all the instrument-based metrics. Furthermore, all four instrument-based metrics failed to reflect the doubling of AGC between R12 and RF, suggesting their inability to register further increases in forest structural complexity, beyond canopy closure.

It is interesting to note that correlation of conventional metrics with all instrument-based metrics declined with increasing information content of the conventional metrics i.e. TSD correlated most strongly with all four instrument-based metrics, followed by BA, with AGC correlating most weakly (Fig. 8a). This may have been because potential sources of variability increase with information content. This assertion was supported by calculating the coefficients of variation (CV) from the data in Table 2 (standard deviation expressed as a percentage of the mean, Table S3). CVs for conventional metrics were highest for AGC and lowest for TSD, consistently across all 3 forested sites.

The most common sources of potential error in field measurements included determining if trees on the perimeter of the circular sample plots should be counted in or not, and the difficulty of seeing tree tops for height measurements in R12 and RF, where high canopy density obscured the view. Field surveys are costly, due to high labour and transport requirements. Furthermore with the large teams of surveyors, required, trampling of young tree seedlings is inevitable, potentially impeding future understory development and carbon absorption.

# 4.3. Recovery of forest structural complexity by the framework species method

Fig. 9 shows visually how effective the FSM is at restoring forest structure over the first decade following initial implementation.

The data, presented above, verify and quantify this visible recovery

of forest structure. Planting of framework tree species augmented natural regeneration, to achieve an initial stocking density of 3100 stems/ ha, mostly of saplings 30-60 cm tall. However, the TSD metric, included only those saplings and trees that had survived and grown large enough to attain a GBH of 5 cm of more by the survey time. By  $1\frac{1}{2}$  years, the R22 mean values of TSD, BA and AGC amounted to 32.7 %, 16.9 % and 9.2 % of the mean reference-forest (RF) values (all significantly lower, P < 0.05, Table 2)—due almost entirely to a few remnant forest trees that remained on the site at planting time. However, by 11½ years, the R12 mean values of TSD, BA and AGC had increased to 81.3 %, 73.3 % and 47.9 % of the mean RF values respectively. R12 values of TSD and BA were statistically indistinguishable from RF values. However, mean AGC in the R12 plot remained significantly lower than the RF value. The result for mean AGC was remarkably close to that from another study of carbon accumulation during restoration of evergreen forest above Ban (=village) Mae Sa, 10 km to the south-east, at the same elevation also using the FSM. In that study, mean tree carbon accumulated in 12-yearold restoration plots was 49 % of the mean reference forest value (FORRU-CMU, 2025). The close reproducibility of the result strongly suggests that during application of the FSM, carbon accumulation lags behind other metrics of structural development, with instrument-based canopy metrics approaching reference-forest values earlier than measurements of forest-carbon.

### 5. Conclusions

In conclusion, the hypothesis that forest canopy metrics, measured by the four instrument-based techniques listed above, could be used to monitor and differentiate states of restoration of upland evergreen-forest in northern Thailand was only partially supported. Whilst all instrument-based techniques successfully distinguished among early restoration stages, once canopy closure reached about 85–90 %, they failed to distinguish further progression towards reference forest conditions. This conclusion was also supported by the fact that correlations between instrument-based and conventional metrics weakened with increasing forest structural development.

Of the four instrument-based metrics tested in our study, we recommend CC\_D as the most cost-effective indicator of forest structural development, up until the point of canopy closure, for the following reasons:

- 1. It distinguished among CT, R22, and R12 almost as well as the other metrics (Table 2).
- It correlated well with other instrument-based metrics across all plots.

- 3. It showed comparable strength of correlation with conventional metrics (r = 0.58-0.77; Fig. 8a).
- A single person can operate it, thus minimizing trampling of seedlings.
- 5. It is simple to use with minimal training.
- 6. Results are immediate, with no need for complex post-processing.
- 7. Its cost is only a fraction of that of the other instruments evaluated.

Beyond canopy closure, however, AGC derived from manual tree measurements, remains the most reliable indicator of forest structural development, combining direct measurements of tree size and wood density with stocking density. However, the high labour requirement and high cost of carbon surveys, and their potential impact on understorey development, remain as strong deterrents to its widespread use.

There remains a need for more reliable and cost-effective methods to track carbon accumulation and structural development during forest-ecosystem restoration. To avoid damaging the forest understory through ground surveys, above-canopy indices, derived from drone imagery aerial LiDAR, may offer the best solution (Spiers et al., 2025).

#### **Funding**

This research was funded by FORRU-CMU's Small-Grant Support for Student Projects. The APC was funded by FORRU-CMU Research Group.

#### CRediT authorship contribution statement

Waiprach Suwannarat: Writing – review & editing, Writing – original draft, Visualization, Software, Methodology, Investigation, Formal analysis, Data curation, Conceptualization. Stephen Elliott: Writing – review & editing, Writing – original draft, Validation, Supervision, Resources, Methodology, Funding acquisition, Formal analysis. Worayut Takaew: Resources, Project administration, Investigation. Pornpawee Laohasom: Investigation, Data curation. Watit Khokthong: Writing – review & editing, Writing – original draft, Visualization, Validation, Supervision, Software, Resources, Project administration, Methodology, Formal analysis, Data curation, Conceptualization.

## **Declaration of competing interest**

The authors declare the following financial interests/personal relationships which may be considered as potential competing interests: Watit Khokthong reports financial support and article publishing charges were provided by Chiang Mai University. Stephen Elliott reports financial support and article publishing charges were provided by Chiang Mai University. If there are other authors, they declare that they have no known competing financial interests or personal relationships that could have appeared to influence the work reported in this paper.

### Acknowledgments

We thank Jutamas Jongman, Chadapohn Tashingkam, Sirui Tao and Woranart Yarangsee for helping with field work and Maxime Réjou-Méchain who provided training in LiDAR processing.

### Supplementary materials

Supplementary material associated with this article can be found, in the online version, at doi:10.1016/j.tfp.2025.100928.

# Data availability

See supplementary material

#### References

- Atkins, J.W., Bohrer, G., Fahey, R.T., Hardiman, B.S., Morin, T.H., Stovall, A.E.L., Zimmerman, N., Gough, C.M., 2018. Quantifying vegetation and canopy structural complexity from terrestrial LiDAR data using the forestr R package. Methods Ecol. Evol. 9, 2057–2066. https://doi.org/10.1111/2041-210X.13061.
- Beckschäfer, P., 2015. Hemispherical 2.0 Batch processing Hemispherical and Canopy Photographs With ImageJ – User Manual, Chair of Forest Inventory and Remote Sensing, Georg-August-Universität Göttingen, Germany.
- Beckschäfer, P., Seidel, D., Kleinn, C., Xu, J., 2013. On the exposure of hemispherical photographs in forests. iForest - Biogeosciences For. 6, 228–237. https://doi.org/ 10.3832/ifor0957-006.
- Bettinger, P., Boston, K., Siry, J.P., Grebner, D.L., 2017. Valuing and characterizing forest conditions. Forest Management and Planning, 2nd Edition. Academic Press, pp. 21–63.
- Černý, J., Pokorný, R., Haninec, P., Bednář, P., 2019. Leaf area index estimation using three distinct methods in pure deciduous stands. J. Vis. Exp. (150). https://doi.org/ 10.3791/59757, 2019 Aug 29.
- Chave, J., Réjou-Méchain, M., Búrquez, A., Chidumayo, E., Colgan, M.S., Delitti, W.B.C., Duque, A., Eid, T., Fearnside, P.M., Goodman, R.C., Henry, M., Martínez-Yrízar, A., Mugasha, W.A., Muller-Landau, H.C., Mencuccini, M., Nelson, B.W., Ngomanda, A., Nogueira, E.M., Ortiz-Malavassi, E., Pélissier, R., Ploton, P., Ryan, C.M., Saldarriaga, J.G., Vieilledent, G., 2014. Improved allometric models to estimate the aboveground biomass of tropical trees. Glob. Change Biol. 20, 3177–3190. https://doi.org/10.1111/gcb.12629.
- Chianucci, F., Macfarlane, C., Pisek, J., Cutini, A., Casa, R., 2015. Estimation of foliage clumping from the LAI-2000 Plant Canopy Analyser: effect of view caps. Trees 29, 355–366. https://doi.org/10.1007/s00468-014-1115-x, 20147.
- Dassot, M., Constant, T., Fournier, M., 2011. The use of terrestrial LiDAR technology in forest science: application fields, benefits and challenges. Ann. For. Sci. 68, 959–974. https://doi.org/10.1007/s13595-011-0102-2.
- Ehbrecht, M., Schall, P., Ammer, C., Seidel, D., 2017. Quantifying stand structural complexity and its relationship with forest management, tree species diversity and microclimate. Agric. Meteorol. 242, 1–9. https://doi.org/10.1016/j. aerformet.2017.04.012.
- Elliott, S., Tucker, N.I.J., Shannon, D., Tiansawat, P., 2022. The framework species method—Harnessing natural regeneration to restore tropical forest ecosystems. Phil. Trans. R. Soc., B37820210073 https://doi.org/10.1098/rstb.2021.0073.
- Elliott, S.D., Blakesley, D., Hardwick, K., 2013. Restoring Tropical Forests: a Practical Guide. Royal Botanic Gardens, Kew, p. 344. https://www.forru.org/library/0000152
- FAO, 2024. RESULT Asia-Pacific: Restoring and Sustaining Landscapes Together A Regional Programmatic Framework For Forest and Landscape Restoration. Food and Agriculture Organization of the United Nations, Rome, p. 79.
- FORRU-CMU, 2025. unpublished report. Chiang Mai University, Thailand. https://www.forru.org/projects/the-bkind-project-supporting-forest-ecosystem-restoration-in-the-upper-mae-sa-valley. accessed on 15th April 2025.
- Gann, G.D., McDonald, T., Walder, B., Aronson, J., Nelson, C.R., Jonson, J., Hallett, J.G., Eisenberg, C., Guariguata, M.R., Liu, J., et al., 2019. International principles and standards for the practice of ecological restoration. Second edition Restor. Ecol. 27, S1–S46. https://doi.org/10.1111/rec.13035.
- Chapter 4 Gilmor, D., 2007. Applying an adaptive management approach in FLR. In: Reitbergen-McCraken, J., Maginnis, S., Sarre, A. (Eds.), The Forest Landscape Restoration Handbook. Earthscan, London, pp. 29–37.
- Huete, A.R., 2012. Vegetation indices, remote sensing and forest monitoring. Geogr. Compass. 6, 513–532. https://doi.org/10.1111/j.1749-8198.2012.00507.x.
- Jantawong, K., Elliott, S., Wangpakapattanawong, P., 2017. Above-ground carbon sequestration during restoration of upland evergreen forest in northern Thailand. Open J. For. 7, 157–171. https://doi.org/10.4236/ojf.2017.72010.
- Jantawong, K., Kavinchan, N., Wangpakapattanawong, P., Elliott, S., 2022. Financial analysis of potential carbon value over 14 years of forest restoration using the framework species method. Forests 13, 144. https://doi.org/10.3390/f13020144.
- Jennings, S., Brown, N., Sheil, D., 1999. Assessing forest canopies and understorey illumination: canopy closure, canopy cover and other measures. Forestry 71, 59–73. https://doi.org/10.1093/forestry/72.1.59, 1999.
- Khokthong, W., Zemp, D.C., Irawan, B., Sundawati, L., Kreft, H., Hölscher, D., 2019. Drone-based assessment of canopy cover for analyzing tree mortality in an oil palm agroforest. Front. For. Glob. Change 2, 12. https://doi.org/10.3389/ffgc.2019.00012.
- Liang, X., Kankare, V., Hyyppä, J., Wang, Y., Kukko, A., Haggrén, H., Yu, X., Kaartinen, H., Jaakkola, A., Guan, F., et al., 2016. Terrestrial laser scanning in forest inventories. ISPRS. J. Photogramm. Remote Sens. 115, 63–77. https://doi.org/ 10.1016/j.isprsiprs.2016.01.006.
- Liu, B., Bu, W., Zang, R., 2023. Improved allometric models to estimate the aboveground biomass of younger secondary tropical forests. Glob. Ecol. Conserv. 41, e02359. https://doi.org/10.1016/j.gecco.2022.e02359, 2023.
- Loffredo, N., Sun, X., Onda, Y., 2016. DHPT 1.0: new software for automatic analysis of canopy closure from under-exposed and over-exposed digital hemispherical photographs. Comput. Electron. Agric. 125, 39–47. https://doi.org/10.1016/j. compag.2016.04.028.
- Maxwell, J.F., Elliott, S., 2001. Vegetation and Vascular Flora of Doi Sutep-Pui National Park, Chiang Mai Province, Thailand. Thai Studies in Biodiversity 5. Biodiversity Research & Training Programme, Bangkok, p. 205. https://www.forru.org/library/ 0000027
- Pati, P.K., Kaushik, P., Khan, M.L., Khare, P.K., 2022. Allometric equations for biomass and carbon stock estimation of small diameter woody species from tropical dry

- deciduous forests: support to REDD+. Trees. For. People 9, 100289. https://doi.org/10.1016/j.tfp.2022.100289.
- Pothong, T., Elliott, S., Chairuangsri, S., Chanthorn, W., Shannon, D.P., Wangpakapattanawong, P., 2022. New allometric equations for quantifying tree biomass and carbon sequestration in seasonally dry secondary forest in Northern Thailand. New For. 53, 17–36. https://doi.org/10.1007/s11056-021-09844-3.
- Pretzsch, H., Río, M.d., Biber, P., Arcangel, C., Bielak, K., Brang, P., Dudzinska, M., Forrester, D.I., Klädtke, J., Kohnle, U., et al., 2019. Maintenance of long-term experiments for unique insights into forest growth dynamics and trends: review and perspectives. Eur. J. Res. 138, 165–185. https://doi.org/10.1007/s10342-018-1151-y, 2019.
- Roussel, J.-R., Auty, D., Coops, N.C., Tompalski, P., Goodbody, T.R.H., Meador, A.S., Bourdon, J.-F., Boissieu, F.d., Achim, A., 2020. lidR: an R package for analysis of airborne laser scanning (ALS) data. Remote Sens Env. 251, 112061. https://doi.org/ 10.1016/j.rse.2020.112061, 2020.
- Russavage, E., Thiele, J., Lumbsden-Pinto, J., Schwager, K., Green, T., Dovciak, M., 2021. Characterizing canopy openness in open forests: spherical densiometer and canopy photography are equivalent but less sensitive than direct. J. For. 119, 130–140. https://doi.org/10.1093/jofore/fvab046.
- Sacco, A.D., Hardwick, K.A., Blakesley, D., Brancalion, P.H.S., Breman, E., Rebola, L.C., Chomba, S., Dixon, K., Elliott, S., Ruyonga, G., et al., 2021. Ten golden rules for reforestation to optimize carbon sequestration, biodiversity recovery and livelihood benefits. Glob. Chang. Biol. 27, 1328–1348. https://doi.org/10.1111/gcb.15498.
  SCENE, 2022. FARO Focus Laser Scanners Training Workbook, 2022.
- Schneider, C.A., Rasband, W.S., Eliceiri, K.W., 2012. NIH Image to ImageJ: 25 years of image analysis. Nat. Methods 9, 671–675. https://doi.org/10.1038/nmeth.2089.
- Seidel, D., Fleck, S., Leuschner, C., Hammett, T., 2011. Review of ground-based methods to measure the distribution of biomass in forest canopies. Ann. For. Sci. 68, 225–244. https://doi.org/10.1007/s13595-011-0040-z.

- Shono, K., Cadaweng, E.A., Durst, P.B., 2007. Application of assisted natural regeneration to restore degraded tropical forestlands. Restor. Ecol. 15, 620–626. https://doi.org/10.1111/j.1526-100X.2007.00274.x.
- Spiers, A.I., Scholl, V.M., McGlinchy, J., Balch, J., Cattau, M.E., 2025. A review of UAS-based estimation of forest traits and characteristics in landscape ecology. Landsc. Ecol. 40, 29. https://doi.org/10.1007/s10980-024-01991-0.
- Suwannarat, W., Suwanprasert, S., Pothong, T., Kullasoot, S., Sapewisut, P., Kasithikasikham, R., Phalaraksh, C., Khokthong, W., Sareein, N., 2024. Forest carbon estimation using two vegetation structural indices derived from terrestrial laser scanner: vegetation area index and leaf area index. Chiang Mai J. Sci. 51 (6). https:// doi.org/10.12982/CMJS.2024.101.
- Taheriazad, L., Moghadas, H., Sanchez-Azofeifa, A., 2019. Calculation of leaf area index in a Canadian boreal forest using adaptive voxelization and terrestrial LiDAR. Int. J. Appl. Earth. Obs. Geoinf. 83. https://doi.org/10.1016/j.jag.2019.101923.
- Torralba, J., Carbonell-Rivera, J.P., Ruiz, L.Á., Crespo-Peremarch, P., 2022. Analyzing TLS scan distribution and point density for the estimation of forest stand structural parameters. Forests. 13 (12), 2115. https://doi.org/10.3390/f13122115.
- UN Decade on Restoration, (n.d.). The UN Decade on Restoration. https://www.decadeonrestoration.org/(accessed on 2nd February 2025).
- Weiss, M., Baret, F., 2017. Can\_Eye v6.4.91 User Manual-2017, p. 56.
- Zanne, Amy E., Lopez-Gonzalez, G., Coomes, David A., et al., 2009. Data From: Towards a Worldwide Wood Economics Spectrum [Dataset]. Dryad. https://doi.org/10.5061/ dryad.234.
- Zhang, J., Wang, J., Cheng, F., Ma, W., Liu, Q., Liu, G., 2023. Natural forest ALS-TLS point cloud data registration without control points. J. For. Res. 34, 809–820. https://doi.org/10.1007/s11676-022-01499-w.